Longitudinal Stability with, and Higher-Order Mode Damping of, Superconducting Storage Cavities in RHIC

N. Towne*

1094 White Oak Lane, Farmington, NY 14425

(Dated: December 31, 2007)

Abstract

Superconducting storage cavities could benefit RHIC by providing better longitudinal confinement of bunches with lower impedance. But there is always the potential for the appearance of instabilities. This study looks at the stability of longitudinal single- and coupled-bunch modes for gold in storage and at transition energy, stability while ramping the cavities to field, and the degree of damping required of the fundamental and higher-order modes to guarantee stability and sufficiently small remnant field during transition jump. Most results were obtained using Vlasov simulations and macro-particle tracking.

*Email: towne56@alumni.uchicago.edu; Work performed under contract number 124117 for Brookhaven Science Associates, LLC under the direction of Ilan Ben-Zvi and Michael Blaskiewicz.

I. INTRODUCTION

There is interest in adding new higher-harmonic cavities (HHCs) to RHIC for a number of reasons [1]. Without attempting to survey these reasons, there are a number of deficiencies of the existing machine in the longitudinal plane that could be improved through the replacement of the cavities. The existing normal-conducting (NC) HHCs for storage are relatively high frequency cavities (197 MHz) [2], into which not all accelerated particles of a bunch can be transferred to a single bucket. There is also significant diffusion of particles out of the buckets, some of which end up in the abort gap. And the NC HHCs have high impedance. In contrast, super-conducting (SC) cavity technology can sustain high voltages requiring fewer cavities, each of which has lower impedance. SC cavities at lower frequency could also capture accelerated bunches each into a single bucket with high efficiency. Finally, SC HHCs potentially have a hefty effect on the performance of stochastic cooling, which directly impacts luminosity [3].

This study addresses basic longitudinal-stability and engineering issues associated with the SC cavities. Longitudinal stability encompasses Robinson or low-mode stability, including higher-order single-bunch coherent modes driven by the high-Q fundamental (accelerating) modes of installed cavities; coupled-bunch (CB) modes driven by both the accelerating mode affecting nearby CB (small $|s|$) modes, and higher-order modes (HOMs) affecting CB modes over which they reside; and stability during storage, acceleration, and, particularly, transition. Damping of the fundamental and HOMs is the tool used to suppress these instabilities, and it is essential to determine the damping of each rf mode of the new SC HHCs needed at each of these energies. Damping of the fundamental is also required to suppress field at the fundamental during transition, which would otherwise push particles out of the bucket or increase the emittance. But more stringently, damping is required at the time when the revolution line nearest the rf line crosses the cavity resonance, at an energy near transition, potentially exciting the $s = +1$ coupled-bunch mode.

So considerable damping of the fundamental of the SC HHCs, and of HOMs, is required during acceleration. After acceleration, when the HHCs are brought to voltage, the damping of the fundamental is removed. During storage, some damping of HOMs must remain. This study looks at these stability issues for 100 GeV/u gold beams during storage and gold at transition energy, and determines the minimum damping required of the rf modes.

Macroparticle tracking and Vlasov simulations were used to determine these thresholds, results of which are reported in Sec. II. Simulations of ramping the SC HHCs to voltage are reported in Sec. III.

At one point there was some discussion of how acoustic noise is mapped to the cavity field and phase. An analytic calculation of this effect for passively driven SC cavities is given in Sec. IV. The negligible damping of these cavities makes the formulas simple.

Finally, results of numerical calculation of the periodic transient associated with impedance in the fundamental modes of the cavities and the abort gap are given in Sec. V. The transient has the effect of shifting the bunches in time, potentially affecting the interaction point. The results show only very small shifts of the order of 10 ps, values that were not unexpected.

Machine parameters used in these calculations are given in Table IV, Table I for gold in storage, and Table II for gold at transition energy. Exceptions to these numbers are given in the text. Frequencies and impedances of longitudinal RF modes of the SC cavities from Superfish (monopole modes only) are given in Table III.

II. COUPLED BUNCH MODE STABILITY

Coupled-bunch modes are driven by impedance overlapping positive harmonics of the synchrotron frequency offset from non-rf revolution lines (upper sidebands). Impedance overlapping lower sidebands damp these modes [4]. RF cavities are often the dominant source of impedance driving these modes. Landau damping via synchrotron frequency spread [5] is a powerful damping mechanism of these modes. In a hadron machine and where there is little synchrotron frequency spread, such as is the case for short bunches in a deep potential well, there is rather little damping and an active feedback system may be required. In RHIC fitted with SC HHCs, it is not clear how much Landau damping is available, and at what magnitude of HOM impedance exists the threshold for instability. This section reports the results of calculations of impedance thresholds of longitudinal coupled-bunch modes in RHIC. Gold beams in storage, and gold at transition energy are treated.

In these calculations, the cavity impedance is modeled as a single HOM centered on the anti-damping sideband, and whose quality factor is set high enough not to overlap the damping sideband. In this way, a worst case threshold for a single HOM is determined. It

does not model the possibility of pile-up of multiple resonances over a single anti-damping sideband, nor does it take into account partial cancellation due to impedance over both damping and anti-damping sidebands.

Values of R/Q for the lowest-lying longitudinal modes are given in Table III. They were calculated by Damayanti Naik using Superfish. There is some sensitivity of the higher modes to details of the shorted end of the cavity, particularly the 1107-MHz mode. So there is some doubt in my mind about the accuracy of Superfish's numbers for those particular modes and that this geometry is somehow pushing the ability of Superfish in some way.

Most of these calculations were performed with a macro-particle tracking code, which tracks particles under the influence of the rf field of the main and HHC cavities, and under the influence of the HOM field. The code was developed for the purpose. It was tested with short gaussian bunches for growth rate against Ref. [4], Eq. 18, and that upper sidebands excite, and lower sidebands damp, instability. Potential well distortion due to a broad-band impedance was not applied.

A few thresholds for Gold in storage were determined through my Vlasov solver [6]. However, the simultaneous long bunches, high HOM frequencies, and small growth rates that characterize RHIC made this code prohibitively slow for most runs. It is practical, however, for a limited number of runs at lower HOM frequencies. Vlasov runs provide a very clean signal for unstable modes, giving precise coherent frequencies and growth rates. As with tracking runs, Vlasov runs at different HOM impedances are extrapolated to the threshold at zero growth rate. When they can be used at all, Vlasov runs are superior to tracking runs for this purpose. In Sec. II A, the ability of Vlasov runs to sort out coupled multipole modes is illustrated.

Machine parameters for these runs are given in Tables IV, I (Au in storage), and II (Au at transition energy). Some calculations for shorter bunches lengths were also calculated and appropriately marked; a set of runs for Gold at transition energy, but with the higher main-cavity field (300 kV) used at least until 2003 [7]. These results are useful to highlight trends.

Error bars in the tracking runs were calculated in some cases with multiple runs to obtain an error bar at each frequency and impedance. Then at each frequency, each impedance was regarded as an independent random gaussian variable. Monte Carlo runs were then used to compute ensembles of least square fits and intercepts, and the mean and standard

deviation were then given as the threshold and error bar. In those cases where a frequency has only single runs at each impedance, each impedance is given the standard deviation of the residual error of about the least square fit of all growth rates at that frequency as its its error bar. Monte Carlo runs proceeded from there. I know this is not rigorous, but this procedure helped me to identify weak data and firm up those data with more runs.

A simple broad-band impedance (BBI) model of the rings was provided by Gang Wang (Table IV). Self-consistent calculation of the potential wells and bunch profiles show that this model has no discernible impact on the bunch profiles of gold in storage due to the deep potential wells provided by the SC HHCs. The BBI does, however, affect the profiles of gold at transition energy. This is due to the fact that the SC HHCs are detuned and damped, and that the main cavities are at low voltage. But even so, the profiles are only slightly lengthened. Figure 1 shows the impact of the BBI on gold at transition energy and in storage with initially gaussian profiles of the appropriate lengths.

The BBM model was not used in any bunch simulation reported here. The self-consistent calculation of profiles converged at about 400 grid points due to the high frequency of the impedance. A similar number of grid points is needed for the Vlasov runs, which is prohibitive given the long simulations required to search for unstable modes.

A. Gold in Storage

For gold in storage, thresholds at a number of frequencies were bracketed by the tracking runs, and three Vlasov-calculated thresholds are also reported. These are collectively plotted in Fig. 2. Thresholds for short bunches (0.26-ns length compared to 2.4 ns) are also plotted in that figure (machine parameters are the same).

For the macro-particle tracking runs, initially gaussian bunches were prepared. For the three Vlasov points, the buckets were initially populated in phase space in proportion to $E^{-\beta/(H_s-H)}$, where H is the hamiltonian, H_s is the value of the hamiltonian on the separatrix, and β is a constant adjusted for the correct bunch length. This phase-space density is not particularly unrealistic, yet has the advantage of going smoothly to zero at the separatrix.

These thresholds are all quite high (except for the short-bunch results), all above 1 MΩ, and do not impose a very tight constraint on HOM damping. Gold at transition energy, it turns out, has lower thresholds. This is due, even though the bunches are longer, to

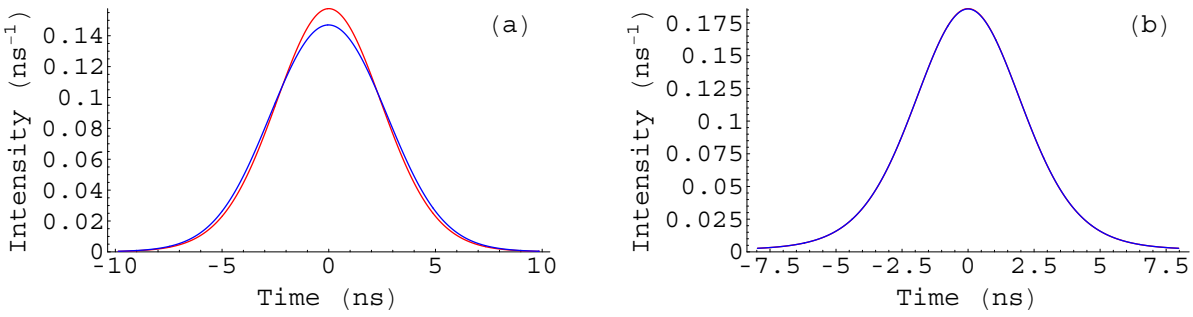

FIG. 1: Bunch profiles of gold at transition energy (a) and in storage (b), without (red) and with (blue) a broad-band impedance model for RHIC provided by Gang Wang. This impedance model is a resonator with $|Z_n|/n = 3.5\ \Omega$, $Q = 1$, and $\omega_r = 2\pi \times 1.7$ GHz, and the undistorted bunch profiles are gaussian.

less Landau damping in the absence of field in the HHCs, which provide more synchrotron frequency spread.

Tracking runs were usually not able to clearly identify the unstable mode. Spectra of the HOM field often show multiple lines of similar height. To check the tracking results, Vlasov runs were used to look in detail at stability at the 168-MHz HOM frequency. Runs at a number of impedances gave precise growth rates at each (Fig. 3a). The highest four impedances were unstable with multipole order $a = 3$ (sextupole mode); the others were unstable with order $a = 2$ (dipole mode). The highest three impedances extrapolated very

TABLE I: Gold in storage.

Parameter	symbol	value	unit
Synchronous energy	T	$= 100$	GeV/u
Revolution frequency	$\omega_0/2\pi$	$= 78.2$	kHz
Main cavity voltage (total)	V_1	$= 300$	kV
SC HHC voltage (total)	V_2	$= 2.5$	MV
Lorentz factor at transition	$\gamma_{\rm t}$	$= 22.3$	
Bunch length	σ_t	$= 2.2$	ns
SC HHC quality factor	$Q_{\rm HHC}$	$= 5 \times 10^8$	(est)
SC HHC detuning	$\Delta\omega_{\rm HHC}$	$= -2\pi \times 151\ s^{-1}$	

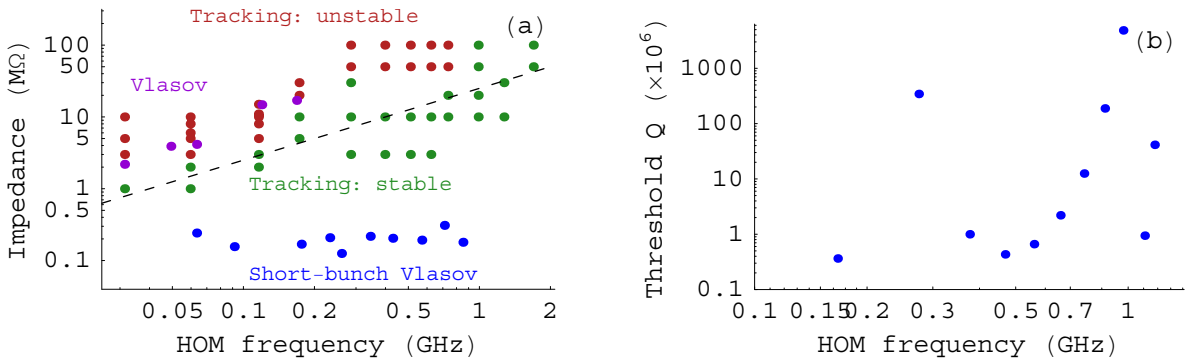

FIG. 2: Impedance thresholds (a) and Q thresholds (b) for gold in storage as a function of HOM frequency. In (a), green points represent stable macro-particle tracking runs, and red points represent unstable macro-particle tracking runs. These points should be regarded as bracketing thresholds. Violet points represent thresholds determined by Vlasov runs. Blue points are thresholds for short (0.26-ns) bunches computed by Vlasov runs. The dashed line proportional to HOM frequency (25 kΩ/MHz) is used to compute the Q thresholds in (b). With the exception of the Vlasov run at 168 MHz, all runs were with the momentum compaction at 0.000865, about half the correct value.

precisely to a sextupole-mode threshold of 34 MΩ. But the fourth $a = 3$ point does not correlate well at all, and seems to be at a transition to the $a = 2$ mode. So I believe that this behavior indicates that the $a = 3$ and $a = 2$ modes are fairly tightly coupled in that transition region, a behavior I had seen in studies of NSLS-II stability [8]. More runs would clarify this.

The analytic form for coherent frequency shifts for gaussian bunches is Eq. 18 of Ref. [4],

$$\Delta\Omega = i\frac{\eta I_{\rm av}\omega_0^2}{2\pi E_0\omega_s}\frac{1}{2^a(a-1)!}(\omega_0\sigma_\tau)^{2a-2}Z_{\rm eff} \tag{2.1}$$

where η is the momentum compaction, E_0 is the total energy, ω_s is the synchrotron frequency, and $Z_{\rm eff}$ is the effective impedance given in Eq. 19 of Ref. [4],

$$Z_{\rm eff} = \sum_{m=-\infty}^{\infty}(mB+s)^{2a-1}Z[(mB+s)\omega_0+\Omega]e^{-((mB+s)\omega_0\sigma_t)^2/2} \tag{2.2}$$

where $s = 0, 1, \cdots, B-1$ is the coupled-bunch mode number, Ω is the frequency of the mode, usually very close to a multiple of the synchrotron frequency, and σ_t is the bunch length. These equations are useful for estimating the multipole-order-dependence of the frequency shift (including growth rate) and, in particular, the slope of the growth rate with respect

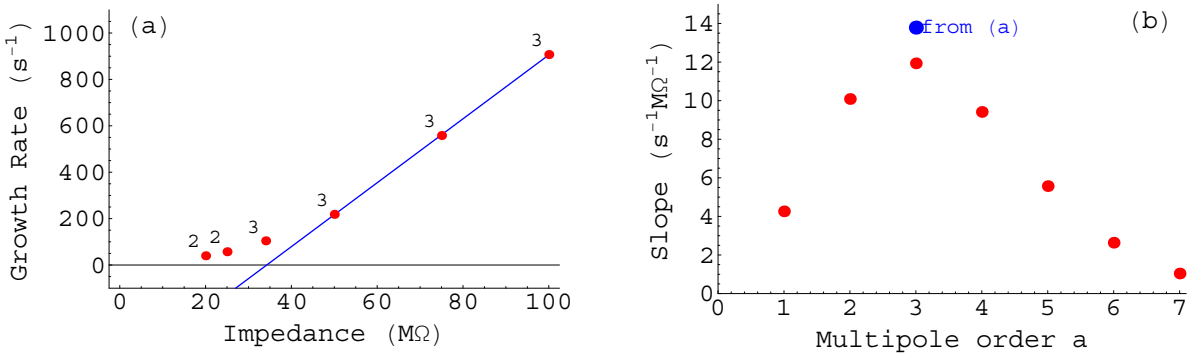

FIG. 3: Growth rates of gold in storage at varying 168-MHz HOM impedances (a), and multipole-order dependence of coherent-frequency shifts of Eq. 18 of Ref. [4] (b). In (a), the points are numbered by the multipole order of the unstable mode as determined by the synchrotron-frequency harmonic of the line in the HOM spectrum. The blue line is a linear fit to the three highest impedance points, precisely indicating an extrapolated threshold of 34.2 MΩ for the $a = 3$ (sextupole) mode, inconsistent with the fourth $a = 3$ point at 34 MΩ. The bunch length is $\sigma_\tau = 2.05$ ns. Plot (b) has the slopes of the imaginary part of Eq. 2.1 (growth rate) as a function of multipole order. The blue point marks the slope of the fit in (a). The momentum compaction used in these runs was 0.0019.

to impedance, plotted in Fig. 3b. That the formula is accurate is shown by comparing the slope of the linear fit of Fig. 3a for the sextupole mode, with Eq. 2.1 in Fig. 3b.

The slope predicted by the formula for the quadrupole mode is not much smaller that for the sextupole mode. Based on that slope and Fig. 3a, the quadrupole threshold can be expected not far from 15 MΩ.

The question that next comes to mind is if the dipole ($a = 1$) mode is unstable at lower impedance where its growth rate would be lower yet. Vlasov and tracking runs become even more lengthy in this regime. Simulations done to date don't show it, but it is still a sensitivity issue.

Note that $Z_{\rm eff}$ is strongly muted at high frequencies, where it is also sensitive to the bunch length, due to the exponential factor in Eq. 2.2.

During the course of the simulations of gold in storage, there were a couple erroneous machine parameters that were carried through to an advanced stage. That the calculations were so lengthy precludes repeating all the runs. The first parameter is the rf field in the

main cavity, which was given the value of 300 kV each cavity, instead of 300 kV total. The three lowest frequencies were rerun. I don't think that the error affects the results significantly for the reason that the total rf field the beam sees is dominated by the SC HHCs, so that the potential well is rather little affected by that 300-kV error. Furthermore, the correct rf potential has more synchrotron frequency spread than the one used, which means that the calculated impedance thresholds are (at least slightly) underestimated.

The second error is more serious, which is that the momentum compaction used in most of the runs was 0.000865, about half the correct value. The 168-MHz Vlasov runs in Fig. 3 are intended to estimate the error in the thresholds introduced by this error. Fortunately there is very little difference between the earlier tracking threshold and this new Vlasov threshold. In fact, the dashed line of Fig. 2 underestimates the thresholds by a greater margin that the uncertainty suggested by the 168-MHz calculation. So the earlier calculation with the error still serves the purpose of conservatively establishing the damping required of the HOMs for gold in storage.

B. Gold at Transition Energy

Growth rates were first calculated for main-cavity field used at the time of commissioning of the current transition-jump method [7], which was 300 kV. Bunch lengths at that time were 1.3 ns, a length that provided less damping of the longitudinal quadrupole mode at the first SC HHC HOM (168 MHz). Since then, the main-cavity field used during that part of the ramp was reduced to 50 kV with bunch lengths at 2.6 ns. Later calculation of thresholds with the lower field shows a threshold Q at the lowest SC-cavity HOM that is much higher—2 k compared to 0.2 k with the shorter bunch. The value of the longitudinal emittance at the start of the transition jump, where the beam is most sensitive to instability, was assumed in these calculations.

Detection of instability and stability in macro-particle runs has been problematic. There is shot noise in these computer runs due to the tracking of particles, so the HOM excitation is necessarily noisy. (I used the HOM field exclusively as a diagnostic.) In runs well above threshold it is easy to see instability; but at lower impedance, it was not obvious when the bunches were stable. So bracketing of the instability threshold does not seem to be generally workable. This was even more difficult at higher HOM frequencies and longer bunches.

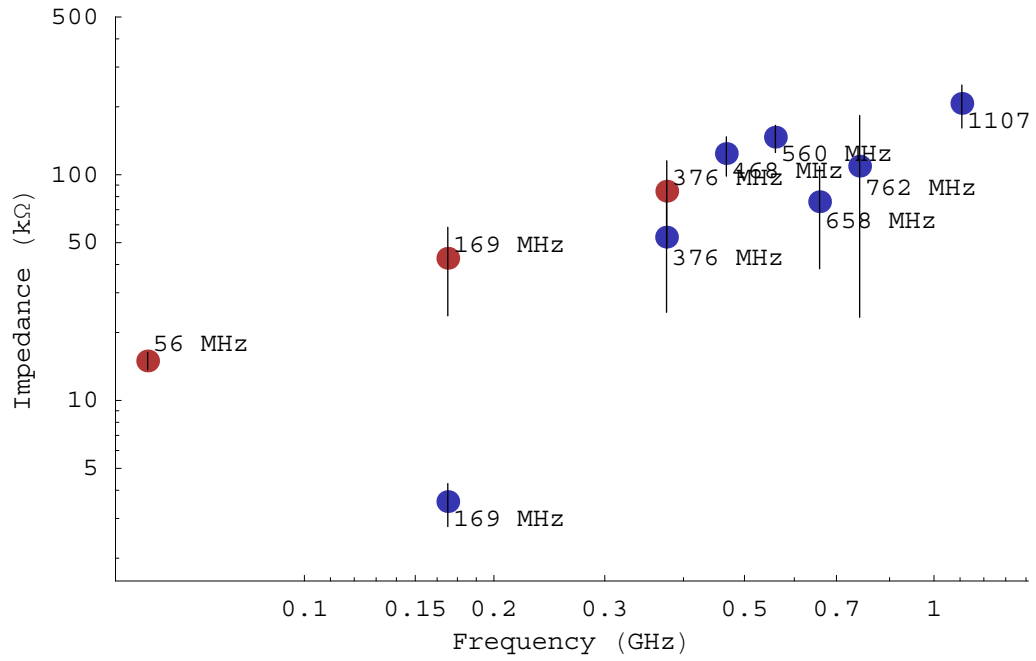

FIG. 4: Impedance thresholds for gold at transition energy as a function of HOM frequency. Blue points are thresholds for 1.3-ns bunches, and red points are for 2.6-ns bunches. See the text for explanation of error bars.

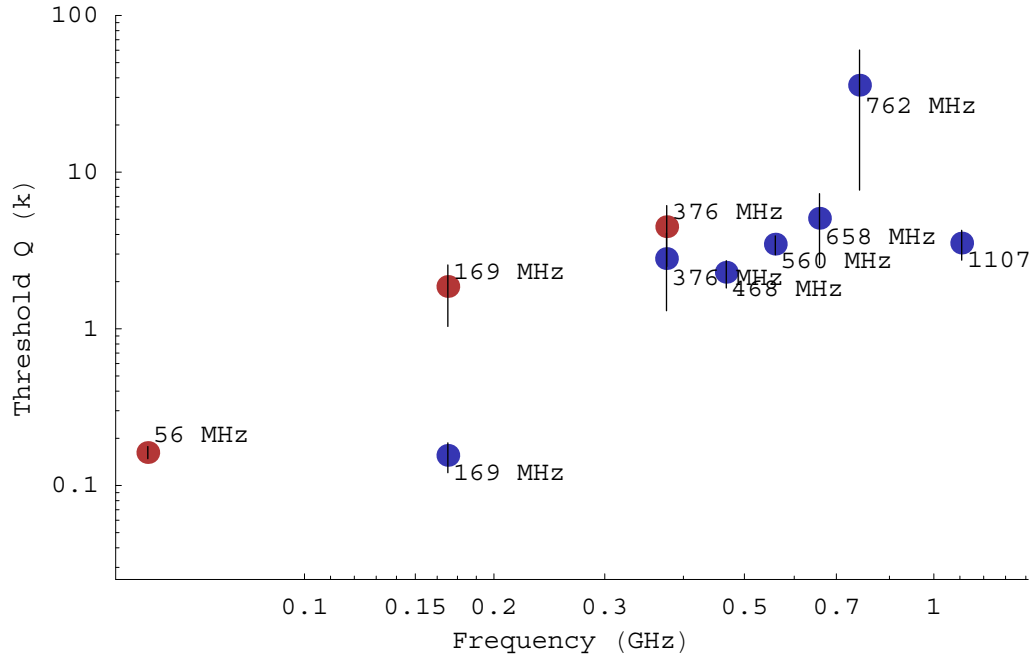

FIG. 5: Q thresholds for gold at transition energy as a function of HOM frequency. Blue points are thresholds for 2.8-ns bunches, and red points are for 1.3-ns bunches. See the text for explanation of error bars.

TABLE II: Gold at transition energy.

Parameter	symbol	value	unit
Synchronous energy	T	$= 21.7$	GeV/u
Main cavity voltage	V_1	$= 50$	kV
Revolution frequency	$\omega_0/2\pi$	$= 78.1$	kHz
SC HHC voltage	V_2	$= 0$	
Momentum compaction	α	$= 5.42 \times 10^{-4}$	
Bunch length	σ_t	$= 2.6$	ns
Longitudinal emittance		$= 0.4$	eV-s (95%)

With shorter bunches where there is a better-defined synchrotron frequency, I was successful fourier analyzing the complex-valued HOM field over individual synchrotron periods. This resulted in mode intensities of all modes at once, some of which could then be plotted as a function of time and growth rates extracted. But with longer bunches and more synchrotron frequency spread, this method is not applicable. There are typically a number of spectral lines of similar intensity present indicating the presence of multiple modes, and time-domain plots of the HOM field show a lot of fluctuation due to interference among these modes. In the end, most of the long-bunch growth rates were extracted from time-domain log plots of the HOM field intensity, in which I looked for an exponential-growth regime and corresponding time constant. Only in some runs was I able to identify a dominant unstable mode.

I also experimented with seeding modes. But without knowledge of details of the unstable modes, it is difficult seed one or a few of these modes preferentially. So that effort was unsuccessful, except for the quadrupole mode at lower frequencies.

Due to these problems, I did not try to compute higher-frequency thresholds for the 2.6-ns bunches at transition energy. It is reasonable to assume that they are higher than those for 1.3-ns bunches, and that they follow the trend of increasing with greater HOM frequency.

C. Coupled-bunch Modes Near the RF Harmonic

The calculations up to this point assume four bunches and an impedance on an anti-damping sideband that by construction does not overlap a damping sideband. So they do not apply to the fundamental mode of an impedance, which is set near an rf harmonic. Such modes are large by design, and in a large ring have significant overlap with nearby revolution lines. Ordinarily, there is a degree of cancellation due to impedance at both the damping and anti-damping sidebands. Due to this cancellation, an unstable nearby mode is not necessarily expected. But during acceleration of a heavy-ion beam in this large ring, the revolution lines move widely relative to the frequency of the unpowered cavities due to the changing speeds of the ions. In fact, it is when the revolution line adjacent to the rf harmonic crosses the cavity resonant frequency that the $s = +1$ CB mode is most strongly excited. So during acceleration this cancellation is spoiled.

In any case, the Vlasov and macro-particle-tracking calculations discussed to this point are not for practical reasons capable of predicting the stability of modes near rf lines in a fill with a large number of bunches.

But they do predict the effective impedance needed to drive a mode to instability. At the frequency of the SC HHC, this threshold impedance is $(nh)^{2a-1} \times 15$ k$\Omega\times$ form factor, where nh is the harmonic number of the SC HHC, shown in Fig. 4, and the form factor is the exponential in Eq. 2.2. So, given the impedance (R/Q) of the fundamental, one can calculate the Q of the fundamental at threshold as a function of cavity detuning. Remember that the cavity detuning during acceleration is dominated by the sweep of the revolution frequency due to the changing velocity of the particles. At transition this detuning is about 52 kHz. As was mentioned earlier, the worst case is expected to be when the detuning is equal to the revolution frequency, i.e., 78 kHz.

The result of this calculation is given in Fig. 6. The cavity is assumed tuned near the final rf frequency. Later, before the beam reaches final energy, the cavity is detuned 10 kHz below the final rf frequency in preparation for reducing the damping and ramping up the rf field. Also plotted is the fundamental mode damping needed to suppress remnant rf field in the cavities during transition jump below its maximum (10 kV total) [2].

The plot shows that keeping the cavity field below the 10-kV limit at transition does not constrain the cavity Q in that the field does not reach the limit even in the $Q \to \infty$

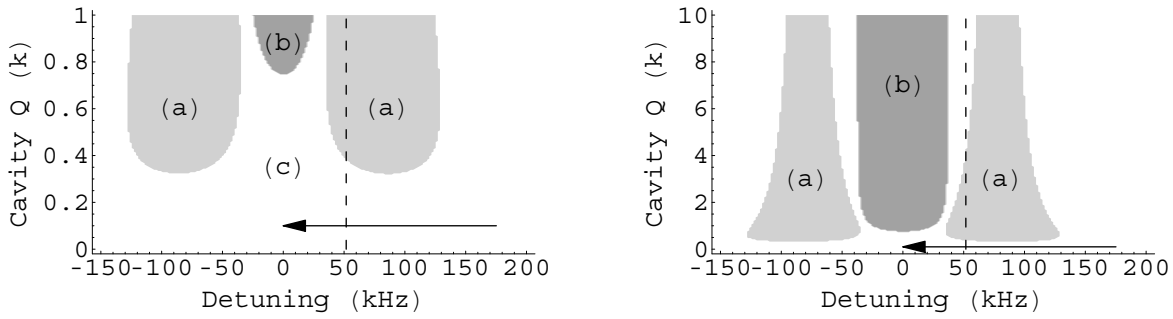

FIG. 6: Stability of $s = \pm 1$ coupled-bunch dipole modes at transition energy in terms of SC HHC main mode Q and cavity frequency relative to the instantaneous cavity detuning $\Delta\omega(t) = \omega_{\rm res} - nh\omega_0(t)$, where $\omega_{\rm res}$ is tuned near the final rf frequency. In regions (a) the $s = \pm 1$ CB mode is unstable. Also plotted is region (b) where the remnant field in the mode is over the 10 kV limit for the transition jump prescribed in Ref. [2]. The sweep of rf frequency during acceleration is denoted by the arrow, and transition itself is denoted by the vertical dashed line. The beam is stable and remnant field is less that 10 kV in regions (c). On the right the vertical scale is expanded $\times 10$. Two SC HHCs per ring are assumed.

limit. Instead, the CB mode stability is the deciding factor, which constrains the Q below a few hundred during acceleration. The lowest threshold occurs around where the nearest non-rf revolution line crosses the cavity resonance, which occurs at $\gamma \simeq 19$, not far from transition where $\gamma \simeq 22$. The scaling of the growth rate in Eq. 18 of Ref. [4] with energy and synchrotron frequency suggests that above transition, the threshold Q may be progressively higher than is indicated by this calculation at $\gamma \simeq 22$, which has that above $\gamma = 30$ the Q is not constrained at all.

Stability of CB modes driven by the NC HHC is not particularly relevant to this study. Its calculation does, however, serve as a sanity check of the SC HHC calculation and I include the results for completeness. Frequency scans of the damped NC cavity show two split modes (Fig. 7a): the impedance is quite a lot larger at rf harmonics about 1.5-MHz offset each way, compared to at the rf harmonic. In the tracking runs, it is not clear exactly which multipole mode is first unstable, although Vlasov runs clearly show that it is $a = 3$. In Fig. 7b is plotted the effective impedance of the NC HHC fundamental for the third multipole ($a = 3$) mode for both 1.3-ns bunches with $V_1 = 300$ kV [7], and 2.6-ns bunches with $V_1 = 50$ kV. They are compared with the threshold, 45 kΩ (Fig. 4), at about that

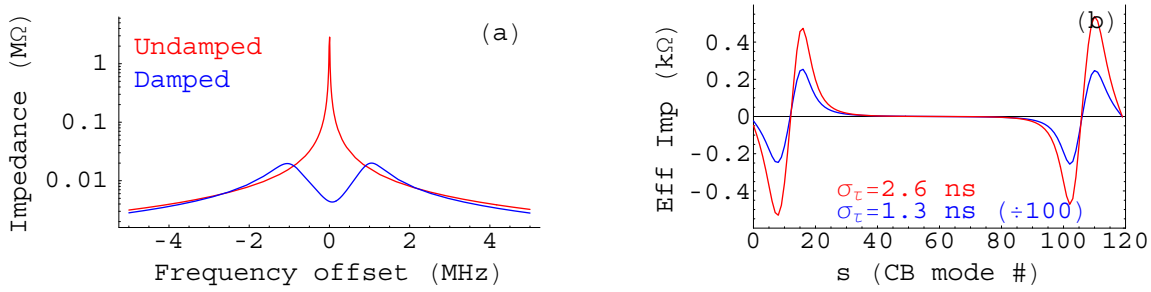

FIG. 7: Undamped and damped NC storage cavities' impedance as a function of frequency offset (a), and effective impedance as a function of CB mode number s (Eq. 2.2) for the third ($a = 3$) multipole mode (b). In (b), the two bunch lengths are determined by different main-cavity fields used during acceleration at different times in the machine's life (see Table II and Ref. [7]). By effective impedance is meant $Z_{\rm eff}/(nh)^{2a-1}$, where nh is the harmonic number of the cavity.

frequency. That the effective impedances are as small as they are is due to the long bunches and the gaussian form factor in Eq. 2.2.

III. RAMPING UP THE CAVITY Q AND FIELDS

After acceleration, the rf-cavity damping and frequencies must be brought to their values for operation in storage. The resonant frequencies of all HHCs are crossed by their rf lines during acceleration, which requires that they be damped at the crossing. Here it is assumed that they will be damped until final energy, at which time the damping is removed while still detuned, and then cavities are tuned and powered (in the case of the NC HHC) to bring the cavities to voltage. Zero-mode stability throughout this time must be ensured. Single-bunch tracking runs were used to simulate this process.

Since the main cavities are powered, they require a source current distinct from the beam. While ramping down the damping of the SC HHC, the beam was found to be unstable. A simple feedback scheme for main-cavity tuning, level, and phase was used to stabilize it during this time. While ramping up the SC HHC field, this scheme became unstable, requiring it to be switched off. Figure 8 shows the field intensity of the main and SC HHCs while bringing up the SC HHCs. The SC HHC detuning was ramped in such a way to linearly ramp the voltage. The detuning started at -10 kHz and ramped to -200 Hz. The bunch is compressed by a factor of two.

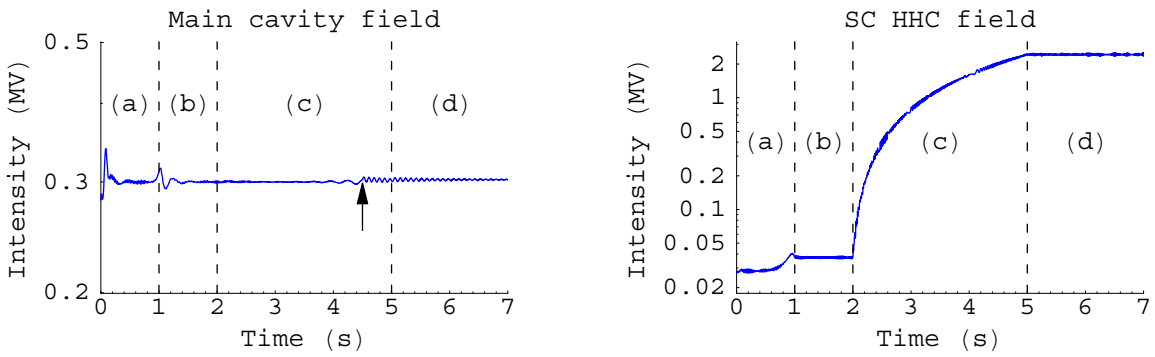

FIG. 8: Simulated main cavity (left) and SC HHC (right) field intensities as a function of time while the SC HHC is brought to voltage, simulated by macroparticle tracking. During period (a), the damping of the SC HHC is being reduced to its operating value, and during period (c) the cavity detuning is being reduced to its nominal value. During periods (b) and (d) there is no change. The arrow in (a) indicates the point at which the main-cavity servos were switched off. The NC HHCs are switched off and damped with the damped impedance of Fig. 7a. 1000 macroparticles were used in the simulation.

Figure 8 shows phaser plots of the main-cavity and SC-HHC fields during the ramps. Both main and SC-HHC phasers are nominally imaginary for bunch confinement (the synchronous phase is assumed zero). The plots show significant shot noise and transients associated with transitions between the different phases of the ramp. That the SC HHC phaser trend deviates from this nominal phase ($+90°$) is due to a small error in the main-cavity generator-current intensity and phase, which shifts the bunch phase from the nominal. This shift is not significant.

While the NC HHCs remain in the rings, there is the option to ramp them to voltage as well. Bringing up the voltage is, like with the SC cavities, a two step process of reducing the damping, followed by reducing the detuning, with the difference that the rf power is brought up with the detuning ramp. Due to the complexity of the damped impedance (Fig. 7), it is not possible to know in detail how the damping is reduced by removal of the loading probe(s). For this reason, I did not try to simulate beam while the damping is reduced. Instead, I started with the cavities at their undamped Q and simulated while the detuning was reduced from -35 kHz, where the cavity field is 8 kV (without rf power applied), to -1.5 kHz. (These figures are total for the seven cavities.) The cavities have a 400-kHz tuning

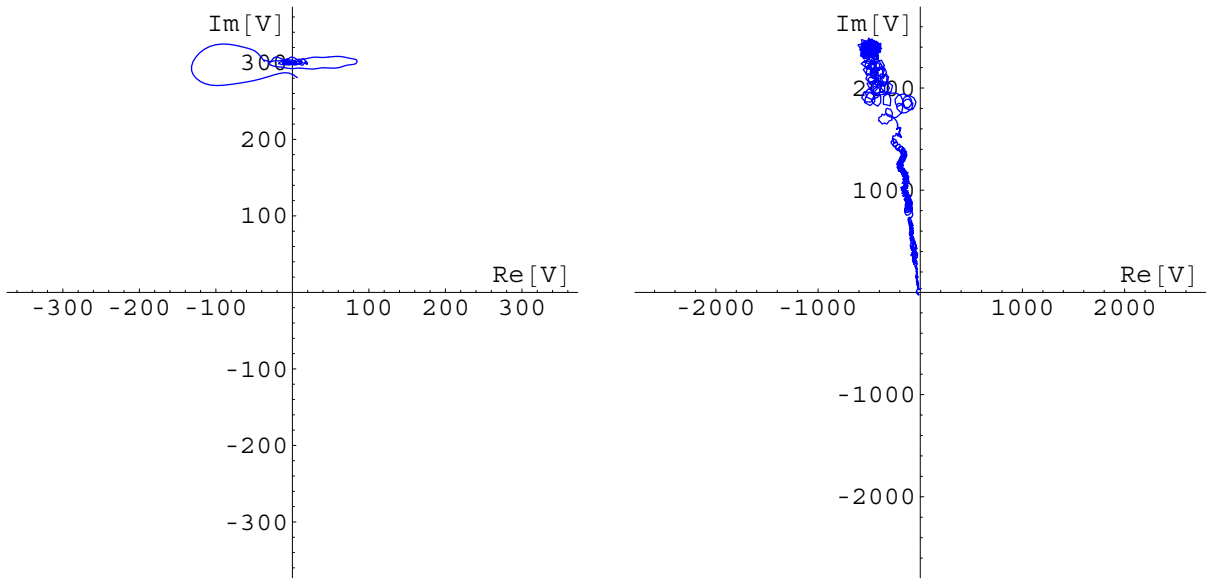

FIG. 9: Simulated main cavity (left) and SC HHC (right) field phasers while the SC HHC is brought to voltage, simulated by macroparticle tracking. The NC HHCs are switched off, detuned, and with the damped impedance of Fig. 7a. 1000 macroparticles were used in the simulation.

range.

But early on I encountered a problem that tracking (and stochastic-cooling) people no doubt know very well. The impedance of the seven NC HHCs is quite large because of the number of cavities and the impedance of each. Beam loading in the cavities is, however, greatly reduced due to the long bunches and the high frequency of the cavity, i.e., the form factor $e^{-(nh\omega_0\sigma_\tau)^2/2}$ for a gaussian bunch is quite small. Even without coherent motion, with a modest number of macroparticles, shot noise in the beam is picked up by the cavity very efficiently and heats the beam quickly. I don't know the parametric dependence of this effect, but a large number of macroparticles is needed to reduce the magnitude of this problem, more that I had been using for simulations with the NC HHC damped. With the NC HHCs undamped, it seems that the heating of the beam requires a prohibitively large number of macroparticles to get realistic behavior of the bunch. So this simulation was not completed.

IV. FIELD FLUCTUATIONS DUE TO MICROPHONICS IN A PASSIVELY DRIVEN SUPERCONDUCTING CAVITY

The presence of microphonic detuning of an SC cavity inevitably introduces variation of the field intensity and phase of the cavity. Tolerances in these field fluctuations imply tolerances of the detuning fluctuations. This section relates the latter to the former.

We model the cavity as an L-R-C tank circuit, with the capacitance being time dependent.

$$I(t) = \frac{d}{dt}(C(t)V(t)) + \frac{V(t)}{R} + \frac{1}{L}\int dt\, V(t) \tag{4.1}$$

where $I(t)$ is the beam current, and $V(t)$ is the voltage in the cavity. Differentiating once gives us the differential equation

$$\frac{d}{dt}I(t) = \frac{d^2}{dt^2}(C(t)V(t)) + \frac{1}{R}\frac{dV(t)}{dt} + \frac{1}{L}V(t) \tag{4.2}$$

or

$$\frac{1}{C(t)}\frac{d}{dt}I(t) = \frac{d^2V(t)}{dt^2} + 2\left(\frac{\dot{C}(t)}{C(t)} + \Gamma(t)\right)\frac{dV(t)}{dt} + \left(\omega_{\rm r}(t)^2 + \frac{\ddot{C}(t)}{C(t)}\right)V(t) \tag{4.3}$$

where $\Gamma(t) = 1/2RC(t)$. $C(t)$ is prescribed by

$$C(t) = C_0(1 + \mu\cos\omega_{\rm m}t) \tag{4.4}$$

where $\omega_{\rm m}$ is the frequency of the frequency modulation, and μ its intensity. This implies that

$$\omega_{\rm r}(t)^2 = 1/LC(t) = (\omega_{\rm rf} + \Delta\omega)^2 - 2\,\omega_{\rm rf}\,\delta\omega\cos(\omega_{\rm m}t) + \cdots \tag{4.5}$$

where $\delta\omega = \mu(\omega_{\rm rf} + \Delta\omega)/2 \simeq \mu\omega_{\rm rf}/2$.

To identify useful approximations, we look at the leading order of the perturbative parts of various terms of Eq. 4.3. First note that $\delta\omega/2\pi$ is of order 1 Hz implying that $\mu \sim 10^{-8}$. The perturbative part of the term containing ω_r^2 scales as $\mu\,\omega_{\rm r0}^2\,V_2$. The $\dot{C}/C$ term scales as $\mu\,\omega_{\rm m}\,\omega_{\rm rf}\,V_2$ a factor of $\omega_m/\omega_{\rm rf}$ smaller. The $\ddot{C}/C$ term scales as $\mu\,\omega_{\rm m}^2\,V_2$, smaller still by the same factor. The time-dependent part of the $\Gamma(t)$ term scales as $\mu\,\Gamma_0\,\omega_{\rm rf}\,V_2$, and Γ is small to start with. Finally, the perturbative part of the left-hand side of Eq. 4.3 scales as $\mu\,\Delta\omega\,\omega_{\rm rf}\,V_2$. So the leading term in the microphonic perturbation of the cavity is the time-dependent part of $\omega_{\rm r}(t)^2$. Other terms are smaller by the factors of $\delta\omega/\omega_{\rm rf}$, $\Delta\omega/\omega_{\rm rf}$, or $\omega_{\rm m}/\omega_{\rm rf}$.

In what follows, all other terms are dropped.

$V(t)$ is separated into two terms, the first, $\bar{V}$, describing the steady-state field in the absence of detuning,

$$\dot{I}/C_0 = \ddot{\bar{V}} + 2\Gamma_0\dot{\bar{V}} + (\omega_{\rm rf} + \Delta\omega)^2\bar{V} \tag{4.6}$$

and the second, δV, describes the perturbation.

$$0 = \delta\ddot{V} + 2\Gamma_0\delta\dot{V} + (\omega_{\rm rf} + \Delta\omega)^2\delta V - 2\omega_{\rm rf}\,\delta\omega\,\cos(\omega_{\rm m}t)\,V_2\cos\omega_{\rm rf}t \tag{4.7}$$

Since the cavity is superconducting, the damping Γ_0 is quite small. Although I retain the term in more complete calculations, that $\omega_{\rm rf}$ is many resonance widths from the resonant frequency means that in this case cavity damping does not play a significant role in microphonic noise transfer to the cavity field.

Equation 4.7 is solved directly for the result

$$\delta V(t) = \frac{\delta\omega}{\Delta\omega^2 - \omega_{\rm m}^2}(\Delta\omega\cos(\omega_{\rm m}t)\cos(\omega_{\rm rf}t) - \omega_{\rm m}\sin(\omega_{\rm m}t)\sin(\omega_{\rm rf}t))V_2 \tag{4.8}$$

The first term is in phase with the cavity field: it is amplitude modulation (AM). The second term is at 90 degrees with respect to the field: it is phase modulation (PM). So the peak amplitude and phase modulation intensities in fractional terms are

$$\text{AM} = \frac{\delta\omega\,\Delta\omega}{\Delta\omega^2 - \omega_{\rm m}^2} \tag{4.9}$$

$$\text{PM} = \frac{\delta\omega\,\omega_{\rm m}}{\Delta\omega^2 - \omega_{\rm m}^2} \tag{4.10}$$

Because of the $\cos\omega_{\rm m}t$ and $\sin\omega_{\rm m}t$ factors in the AM and PM responses, respectively, the former response function is real, and the latter is imaginary, in the frequency domain. For reference, $\Delta\omega \simeq 2\pi \times 151$ Hz with two cavities, $\omega_{\rm m}$ is a few tens of Hz, and $\delta\omega$ is expected to be in the 0.1- to 1.0-Hz range. So the principal uncertainty determining the severity of amplitude and phase modulation arising from microphonics is $\delta\omega$.

Another issue is the presence of noise at modulation frequencies ω_m near $\Delta\omega$. The $\Gamma \to 0$ approximation eventually fails, but, because Γ is so small, there is severe amplification before that happens. Note also that with only one SC cavity in each ring, $\Delta\omega$ is half the number given — 75 Hz — assuming the one cavity is to support the full voltage. This smaller number puts the detuning nearer the cavities' population of noisy acoustic resonances.

V. PERIODIC TRANSIENT IN THE CAVITY FIELD DUE TO THE ABORT GAP

By periodic transient I mean the part of the rf voltage in the cavities that is periodic in the revolution period and not having a component at the rf frequency and harmonics. In fourier space, this means revolution lines in the cavity field that are not harmonics of the rf frequency. The potential impact of such a transient is that the interaction points vary with bunch along the bunch trains. This is not a new problem in RHIC. The point of this section is to determine if the SC cavities greatly aggravate such shifts in the interaction points.

Since the rf field in the main cavities as a function of time is nearly linear in time near the synchronous phase, the shift of the synchronous phase due to a perturbation of the field intensity is nearly proportional to the perturbation. This proportionality for the synchronous phase $t_{\rm s}$ expressed in terms of time is

$$dt_{\rm s} \simeq \left.\frac{1}{dV(t)/dt}\right|_{t=0} \times \delta V \tag{5.1}$$

where $V(t)$ is the total rf voltage as a function of time. Above transition, a positive shift of the rf field at the synchronous phase delays the bunch. In storage,

$$\left.\frac{1}{dV(t)/dt}\right|_{t=0} = 1.01 \text{ ps/kV} \tag{5.2}$$

The periodic transient was calculated by simply applying kicks to the cavities at the nominal times of each bunch, given that the ring is filled as given in Table IV and the bunch length as given in Table 2. A bunch form factor of $e^{-(nh\omega_0\sigma_t)^2/2}$ is assumed. Over time, the field in the cavity damps to the periodic field. Since the shifts are so small, there is no need for a self-consistent calculation. When the nearest (non-rf) revolution lines are many resonance widths from the resonant frequency, as is the case for the SC cavities, the resulting behavior is dominated by the reactive part of the impedance and is insensitive to the exact Q to which the cavities are loaded.

For the SC cavities, the field perturbation at the nominal synchronous phase and the resulting shift in synchronous phase are given in Fig. 10. They result in a ± 2 ps shift along the train. For comparison, the shift due to the main cavities is shown in Fig. 11. Finally, also for comparison, the shift due to the NC HHCs when not in the damped state is shown in Fig. 12.

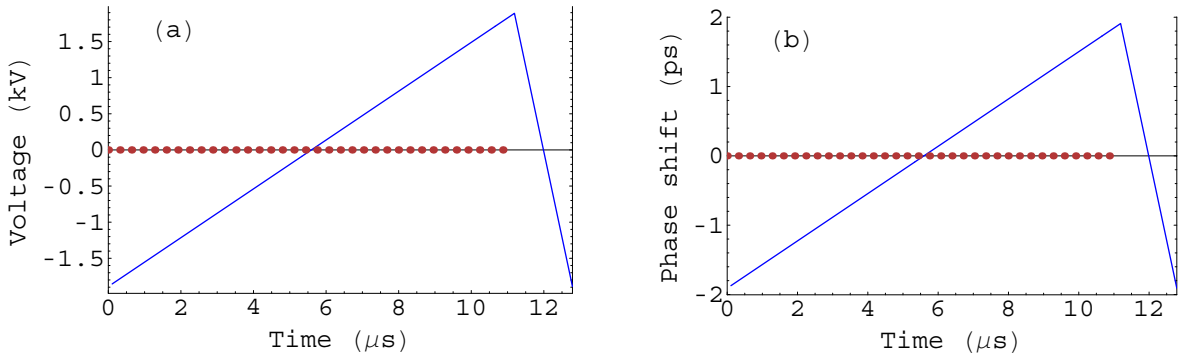

FIG. 10: SC cavity field perturbation (two cavities) at the nominal synchronous phase (a), and the resulting shift in the synchronous phase (b), of each bucket of a turn. For gold in storage.

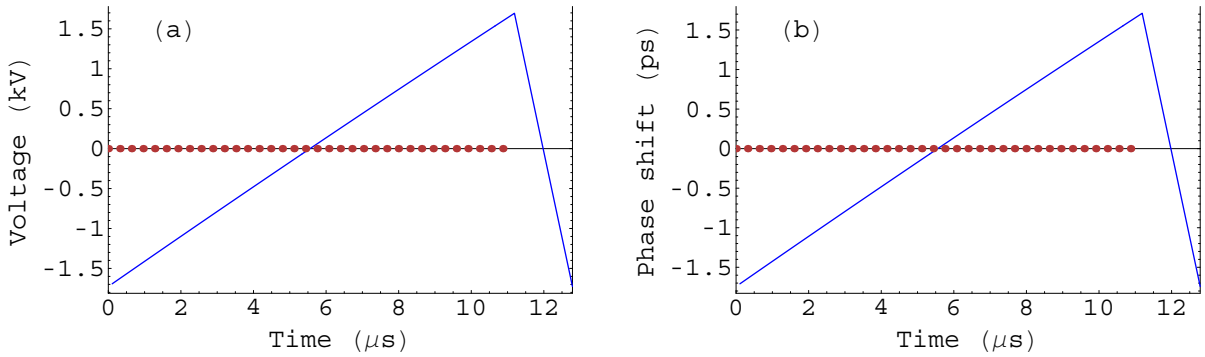

FIG. 11: NC main cavity field perturbation (two cavities) at the nominal synchronous phase (a), and the resulting shift in the synchronous phase (b), of each bucket of a turn. For gold in storage.

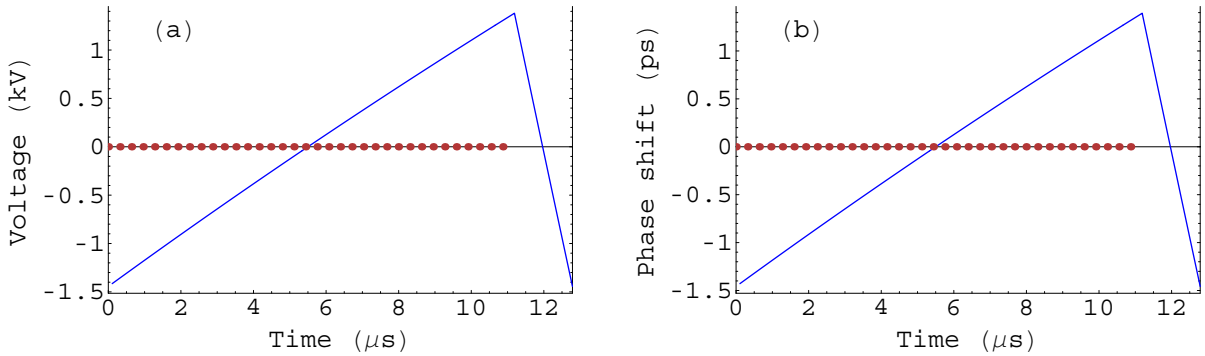

FIG. 12: NC HHC field perturbation (seven cavities) at the nominal synchronous phase (a), and the resulting shift in the synchronous phase (b), of each bucket of a turn. For gold in storage and the cavity undamped.

The shifts are of similar magnitude for all cavities (with the exception of the NC HHC when damped). This occurs even though the R/Qs of the seven NC HHCs is so much larger. What evens the score is the higher frequency of the NC HHCs, which results in a much smaller form factor. Total shifts are the sum of shifts due to the three sets of cavities—around 10 ps total. So this section has been a long winded way to say that the shifts are insignificant.

VI. SUMMARY

Longitudinal CB mode stability constrains the damping of the fundamental and HOMs of the SC HHCs in a few ways. The fundamental must be fairly strongly damped during acceleration to suppress the $s = +1$ CB mode when that revolution line crosses the cavity fundamental mode. This constraint more than meets the requirement that the field in the fundamental at transition be sufficiently small to prevent significant particle loss or emittance growth. Damping of the first HOM is constrained by tracking simulations of CB-mode stability during acceleration to about $Q = 1$ k or less. Damping of higher-frequency HOMs is more relaxed. In contrast, Vlasov and tracking simulations do not significantly constrain HOM damping during storage. Resonance widths can be narrower than revolution line spacing.

Macro-particle tracking simulations were used to check that reducing the damping of the fundamental and ramping up the field of the SC HHCs following acceleration does not present any sort of problem.

An analytic calculation of passively driven SC-cavity intensity and phase modulation driven by cavity frequency modulation returned simple formulas for AM and PM (amplitude and phase modulation) (Eqs. 4.9 and 4.10). The AM and PM formulas relate these quantities to the magnitude of the cavity frequency modulation, the modulation frequency, and the cavity detuning. The zero-cavity-damping approximation fails when the modulation frequency offset is within a few line widths of the cavity resonance, a frequency span that is quite small for passively driven SC cavities. But AM and PM noise can become quite large when noisy acoustic modes approach the cavity resonance.

Finally, a check of synchronous phase shifts of bunches along the train due to the SC HHCs show that they are very much smaller than the bunch lengths, as they have always

been.

REFERENCES

[1] I. Ben-Zvi, *Proposal: 56 mhz rhic srf cavity*, RHIC Retreat (2007), http://www.c-ad.bnl.gov/RHIC/retreat2007/.

[2] *THE CONCEPTUAL DESIGN OF THE RHIC RF SYSTEM*, Tech. Rep. RHIC/RF 22, Brookhaven National Laboratory, Upton, NY 11973 (1994).

[3] M. Blaskiewicz, J. M. Brennan, and F. Severino, *Stochastic cooling of high energy bunched beams*, RHIC Retreat 2007 (2007), http://www.c-ad.bnl.gov/RHIC/retreat2007/.

[4] J. M. Wang (1980), Brookhaven National Laboratory Report No. BNL-51302.

[5] J. M. Wang (1988), presented at the 1988 Joint US-CERN Particle Accelerator School, Capri, Italy, October 19-25, 1988.

[6] N. Towne, Phys. Rev. ST Accel. Beams **4**, 114401 (2001).

[7] C. Montag and J. Kewisch, Phys. Rev. ST Accel. Beams **7**, 011001 (2004).

[8] N. Towne, *Bunch and RF Stability and RF Noise in NSLS-II*, NSLS-II Technical Note 27, For the NSLS-II design effort, 1094 White Oak Lane, (2007).

[9] J. Wei, J. Kewisch, V. Ptitsin, and J. Rose, *RHIC Longitudinal Parameter Revision*, Tech. Rep. RHIC/AP/145, Brookhaven National Laboratory, Upton, NY 11973 (1997).

TABLE III: SC HHC longitudinal modes calculated by Damayanti Naik using Superfish.

Frequency (MHz)	R/Q (Ω)	Frequency (MHz)	R/Q (Ω)
56	46.1	762	1.52
166.9	11.45	866	0.115
275	0.02	970	0.005
376.5	9.42	1073	0
468.4	27.05	1107	29.4
560	21.1	1177	0.71
659	7.48		

TABLE IV: RHIC ring parameters [2, 7, 9], symbols, and values assumed in this study. Some parameter pertain to gold ions.

Parameter	symbol	value	unit
Circumference	cT_0	= 3833.845	m
Longitudinal emittance		$= \sim 0.5$	eV-s (95%)
Gold ions per bunch		$= 10^9$	
Transition	γ_t	= 22.3	
RF buckets	h	= 360	
Buckets potentially filled	B	$= h/3$	
Bunches in fill		= 105	every third bucket
Average beam current	I_{av}	= 104	mA
Broad-band impedance	$\lvert Z_n\rvert/n$	= 3.5	Ω
	ω_{BBI}	$= 2\pi \times 1.7$	GHz
Main cavity impedance	R_0/Q_0	= 63.64	Ω
Main cavity count	n_{cav}	= 2	per ring
Main cavity frequency	f_{rf}	= 28	MHz
Main cavity harmonic	h	= 360	
NC HHC impedance per cell	R_0/Q_0	= 162	Ω
NC HHC count	n_{cav}	= 3	per ring
		+ 4	in common
NC HHC frequency	f_{rf}	= 197	MHz
NC HHC harmonic	nh	= 2520	
SC HHC impedance per cell	R_0/Q_0	= 46.1	Ω
SC HHC count	n_{cav}	= 2	per ring
SC HHC frequency	f_{rf}	= 56	MHz
SC HHC harmonic	nh	= 720	